Plugo: a VLC Systematic Perspective of Large-scale Indoor Localization

Qing Liang and Ming Liu

qing.liang@my.cityu.edu.hk eelium@ust.hk
August 01, 2017

Abstract

Indoor localization based on Visible Light Communication (VLC) has been in favor with both the academia and industry for years. In this paper, we present a prototyping photodiode-based VLC system towards large-scale localization. Specially, we give in-depth analysis of the design constraints and considerations for large-scale indoor localization research. After that we identify the key enablers for such systems: 1) distributed architecture, 2) one-way communication, and 3) random multiple access. Accordingly, we propose *Plugo* — a photodiode-based VLC system conforming to the aforementioned criteria. We present a compact design of the VLC-compatible LED bulbs featuring plug-and-go use-cases. The basic framed slotted Additive Links On-line Hawaii Area (ALOHA) is exploited to achieve random multiple access over the shared optical medium. We show its effectiveness in beacon broadcasting by experiments, and further demonstrate its scalability to large-scale scenarios through simulations. Finally, preliminary localization experiments are conducted using fingerprinting methods in a customized testbed, achieving an average accuracy of $0.14m$ along with a 90-percentile accuracy of $0.33m$.

1 Introduction

Location awareness is critical to many indoor applications [1–3], e.g., way-finding in a metro station, industrial unmanned ground vehicle (UGV) navigation in a warehouse, and location-based services (LBS) in retail. As reported by MarketsandMarkets recently, the global indoor location market is projected to grow to USD 23.13 billion by 2021 [4]. While GPS has effectively solved the ubiquitous localization problem in most outdoor scenarios, a seamless indoor localization solution remains challenging that is capable of providing a comparative user experience to what GPS has done outdoors [3]. It is expected to be accurate, responsive, lightweight, scalable, robust, low-cost and ubiquitous.

Previously, many RF-based localization methods were proposed mainly by the wireless communication community and normally achieved accuracies around several meters owing to the multipath fading effect [5]. Also, decimeter-level accuracies were feasible at the cost of sophisticated hardware components. Meanwhile, approaches like Simultaneously Localization and Mapping (SLAM) [6, 7] along with visual-inertial odometry [8] have been pervasively studied in robotics, since localization is fundamental to many robot problems such as navigation

[9, 10] and path planning [11]. A centimeter-level accuracy could be easily achieved using a laser-based SLAM technique yet at the expense of high sensor cost. Odometry methods are prone to drift and lack global references. An expected indoor localization solution should seek a reasonable balance between the system performance and cost so as to achieve widespread adoptions in large-scale environments. It is believed that VLC-based localization is a promising technology to fill this gap [2, 12].

Unlike conventional RF-based localization methods [13–18] that require multiple dedicated wireless access points (e.g., WiFi ad-hocs and Bluetooth beacons) to communication and localization, VLC-based methods leverage the existing LED lighting infrastructure which already serves its primary function of illumination in most indoor scenarios. In contrast, the inherited benefits are twofold: lower-cost versus better-accuracy. LED lights are gradually replacing the conventional incandescent and fluorescent lighting fixtures thanks to the higher energy-efficiency and longer life-time of high-powered white LEDs, to name a few. We may safely vision that the LED lighting infrastructure will be ubiquitous indoors. From the standpoint of venue owners, the investment is moderate on VLC-compatible LED lights with respect to dedicated wireless beacons in the long run. Besides, a better localization accuracy could be expected as VLC signals are highly directional and immune to multipath fading effects that used to be suffered by RF signals. The dense deployment of lighting fixtures also contributes to better localization performance. In fact, we witness that some giant corporations have devoted to the R&D on this technique, e.g., Qualcomm, Phillips, GE, and Acuity. For instance, Lumicast [3], a state-of-the-art VLC-based localization solution announced by Qualcomm, shows a centimeter-level positioning accuracy at an update rate of 30 Hz on a commercial smartphone. Inspired by these observations, we believe that LED lights shine a promising opportunity to the ubiquitous indoor location service in the near future.

During the last decade, increasing studies on VLC-based localization methods have emerged in the literature. They can be generally divided into camera- and photodiode-based directions with respect to the adopted VLC receivers [12]. Currently, camera-based methods are about to go mainstream in the industry benefiting from the following gains:

1. No extra hardware modification or accessories required on the receiver side since inbuilt front-facing cameras with a megapixel resolution are commonly available in modern smartphones;

2. No dedicated multiple access schemes needed thus simplifying the design of VLC transmitters because cameras are capable of spatial discrimination of clustered lighting fixtures;

3. Providing high-accuracy 3D position and heading information using angle-of-arrival (AOA) localization algorithms as cameras are inherently AOA sensors with millions of tiny “antennas”.

Nonetheless, some intrinsic drawbacks remain unsolved. To be specific, camera-based localization systems impose some of the following constraints on a real use-case:

1. Power-consuming. First of all, the inbuilt camera of a smartphone consumes around 300mW while being kept on during the whole localization

process [19]. Moreover, it is computational demanding to process the acquired high-resolution images leading to more battery drain [1];

2. Relying strictly on a line of sight (LOS) view from densely deployed lighting fixtures. This is subject to the AOA-based algorithm and limited field of view (FOV) of existing front-facing cameras. However, the LOS condition does not always hold;

3. Requiring the registration of all the light beacons with explicit 3D locations. It is a common headache of all the model-based localization methods. The deployment process in a large-scale environment tends to be tedious, labor-intensive, and time-consuming especially when lacking a detailed blueprint with updated configurations of lighting fixtures.

Besides, a salient barrier of photodiode-based methods for commercial deployment is that existing light sensors on smartphones are unsuitable for VLC usage owing to the confined frequency response. Additional multiple access schemes are required to differentiate spatially distributed lights within the sensor FOV due to the lack of spatial discrimination of photodiodes. In addition, localization methods that rely on RSS measurement are vulnerable to the fluctuation of VLC signals due to the ambient disturbance, such as shadowing and reflection. However, photodiode-based methods deserve further investigation owing to the benefits in nature: 1) Energy-efficient thus not draining the battery hard; 2) Lightweight since the signal processing is much simpler than that of camera-based methods; 3) LOS-view independent and free of location registration when using model-free localization methods (e.g., fingerprinting). Previously, a variety of photodiode-based localization systems were proposed through simulation and experiments [20–22], and different kinds of multiple access schemes were introduced [23–25]. Most of these studies evaluated the system performance in a room-size or table-size testbed, while only a few considered the scalability in large-scale scenarios.

To grant reliable localization performance, the end user requires a set of simultaneous observations of multiple light beacons. A fundamental problem is how to achieve reliable beacon broadcasting over the shared light medium on top of commercial LED lights. In this paper, we focus on the beacon broadcasting problems of a photodiode-based localization system aiming at mass deployment in large-scale environments. Stimulated by Epsilon [20] especially the random multiple access scheme, we especially take into consideration the design constraints arising from commercial LED lights with emphasis on the requirements of the large-scale indoor localization.

We propose **Plugo** (named after "Plug and Go") in this paper, a dedicated VLC system which is capable of providing reliable beacon broadcasting over a shared optical medium from multiple LED bulbs to a single photodiode receiver. It deviates from the general VLC systems [26] developed in the wireless communication community that pursues high data throughput along with bidirectional communication. The key differentiation points of Plugo are threefold: 1) distributed architecture, 2) one-way communication, and 3) random multiple access. Compared with our previous work [22, 27], Plugo moves a small step further towards the expected localization technology.

Specifically, we stress our novel contributions as follows:

1. Identifying the key enablers to a photodiode-based VLC system towards large-scale localization through in-depth analysis of the design constraints and considerations;

2. Design, implementation, and evaluation of such a VLC system that is easy to use in a plug-and-go fashion;

3. Implementation of a basic framed slotted ALOHA (BFSA) random multiple access scheme with practical issues taken into account. This is the first experimental demonstration in this community to the best of our knowledge.

The remainder of this paper is organized as follows. Section II discusses from scratch the design constraints and considerations; The detailed system design and implementation are described in Section III and Section IV respectively; Section V demonstrates the evaluation results; Finally, we conclude this paper in Section VI.

2 Design Constraints and Considerations

2.1 Commercial LED lights

LED lights comprise a number of high-powered white LEDs, which can be switched on and off rapidly to convey information via VLC at a high frequency imperceivable to human eyes [26]. The basic principle of VLC is intensity modulation and direct detection (IM/DD). This is because visible light emitted by white LEDs is inherently noncoherent light with a broad spectrum. It is unlikely to modulate either the frequency or phase of visible light itself. The most widely adopted white LED in luminaries is made of a blue LED with a yellow phosphor coating. It is much cheaper and more energy-efficient than the RGB-type LEDs. The typical modulation bandwidth is around 2 MHz which is more than enough for localization purpose [2]. However, there are still some inherent constraints. For example, the color shift keying (CSK) modulation and wavelength division multiple access (WDMA) schemes only work with RGB-type LEDs and thus should be avoided in a system for widespread adoptions. To fulfill the primary illumination function of LED lights, we have to tackle the potential flicker and dimming issues.

2.2 Large-scale Localization

The long-term goal is to build a commercially viable localization system for widespread adoptions in large-scale indoor scenarios with minimized requirements of installation and configuration. We identify the key technical criteria to enable this on the basis of [3] and [5] in the following:

Accurate. It concerns both the accuracy and precision. Normally, the accuracy is measured by the mean distance error while the precision described by the empirical cumulative distribution function (CDF). This is a straightforward requirement of many indoor applications like LBS.

Responsive. It means a short localization latency and a high update rate. This is essential for real-time use cases such as UGV navigation and pedestrian tracking.

Lightweight. It refers to the minimized computational overhead and system complexity along with power consumption. In this way, compelling indoor location services are more likely to be affordable by resource-constrained mobile devices (e.g., smartphones) without draining heavily either the computation resources or battery.

Scalable. The meaning is twofold: 1) scaling to the coverage area and 2) scaling to the user density. In other words, the localization performance should not degrade significantly as the localization scope increases or more users are involved. This is critical to large-scale localization.

Robust. The system could function well in some harsh scenarios, e.g., with some beacons broken abruptly or coming into operation for the first time.

Low-cost. The cost concerns money, time, labor, etc. It is challenging to seek an elegant balance between the performance and the cost.

Ubiquitous. The location service can be generally enabled in most scenarios once required. It is the ultimate goal to provide a ubiquitous indoor location service which is comparable to what GPS has done outdoors.

Beacon broadcasting on top of LED lights founds the basis of a VLC-based localization system. Specially, we focus on a photodiode-based VLC system for localization purpose. In order to develop a VLC system conforming to the technical criteria for the large-scale localization, we give an in-depth discussion of the design considerations from three aspects: network architecture, communication links, and multiple access schemes.

2.3 Centralized vs. Distributed Architecture

For a centralized architecture, beacons are scheduled by a superior coordinator through a wired or wireless backbone network. To grant a strict time synchronization, localization methods based on time-of-arrival (TOA) and time-difference-of-arrival (TDOA) normally require a wired backbone connection among the transmitters [12]. Besides, methods that exploit the time division multiple access (TDMA) also rely on a centralized architecture [28]. However, the backbone network increases the total hardware complexity along with the installation cost. Worse still, a centralized system is prone to collapse once the coordinator is broken. On the contrary, the distributed architecture is free of either a coordinator or a backbone connection. It is likely to provide improved robustness during the operation, reduced hardware complexity and cost during the installation. Many localization systems were proposed in the literature with a distributed architecture [1, 20–22].

2.4 Two-way vs. One-way Communication

From now on, we consider a distributed architecture of the light beacons. As for a broadcasting network, communication between the beacon and mobile user can be either bidirectional or unidirectional. Contention based multiple access schemes can be exploited on top of two-way communication, e.g., Carrier Sense Multiple Access with Collision Avoidance (CSMA/CA). Time synchronization is also feasible so as to favor a time-of-flight (ToF) localization method [5]. Several networked VLC systems were proposed in the communication community that exploited a CSMA/CA-based medium access control (MAC) [29, 30]. From the localization standpoint, however, systems relying on two-way communication

between the infrastructure and the end user do not scale well as the beacons and users increase. This is because the frequent handshake connections in two-way communication burden the total traffic thus involving more interference to other nodes working concurrently. Besides, the hardware complexity along with cost will increase as two-way communication requires VLC transceivers on both the beacon and mobile user sides. To enable large-scale localization, we prefer one-way communication because of the better scalability and reduced hardware complexity as well as cost. In fact, some camera-based commercial localization systems offered by Qualcomm [3] and Phillips [31] support one-way communication only.

2.5 Fixed vs. Random Multiple Access

We now focus on a fully distributed VLC system with one-way communication. Due to the absence of either a backbone network or bidirectional communication, it's no longer possible to perform any synchronization either between each two beacons or between the beacon and the mobile user. To tackle this problem, some asynchronous multiple access schemes have been proposed, e.g., frequency division multiple access (FDMA) [32] and code division multiple access (CDMA) [33]. Normally, a fixed frequency carrier or pseudo-noise sequence is allocated to each light beacon in advance. When it comes to a large-scale environment with thousands of lights, however, the number of frequency carriers or pseudo-noise sequences available are limited to use. Authors in [32] proposed an RF-carrier allocation scheme to mitigate the inter-cell interference by reusing a limited number of carriers in non-adjacent cells. In their context, one had to guarantee that none of any adjacent lights shared the same frequency carrier. It imposed a stringent constraint on the practical deployment, especially in a large-scale environment. Indeed, this is a common problem of many other fixed multiple access schemes (e.g., CDMA), but it has long been overlooked by many researchers.

A radical idea is to dynamically assign a limited number of communication resources (e.g., time slots, frequency carriers, and optical CDMA codes) in a random fashion to all the beacons involved — random multiple access [34]. In this context, every beacon in the VLC system competes with one another equally for communication resources. As a result, the random access scheme is free of the headache suffered by its counterpart. Collisions occur when two different beacons compete for the same piece of resources (e.g., time slots). But this problem can be easily worked out through multiple observations. To the best of our knowledge, Epsilon [20] was the first experimental system in this community that involved random multiple access — channel hopping. A BFSA-based random access scheme was first introduced by Zhang et al [21] and evaluated through simulation. In this paper, we will demonstrate the implementation of this scheme by taking into account practical issues.

3 The Plugo System

The Plugo system, as shown in Figure 1, comprises a set of VLC-compatible LED bulbs as positioning beacons and a photodiode receiver which is attached to the user device (e.g., smartphones, tablets) via an audio jack. The system ar-

chitecture is distributed without any backbone connections among these bulbs. Each bulb broadcasts its unique beacon identity to the receiver by one-way communication over a shared optical channel. The user device equipped with a receiver takes continuous observations of multiple light beacons overhead retrieving each beacon identity along with the corresponding received signal strength (RSS). VLC-based localization is thus feasible on the top of these observations.

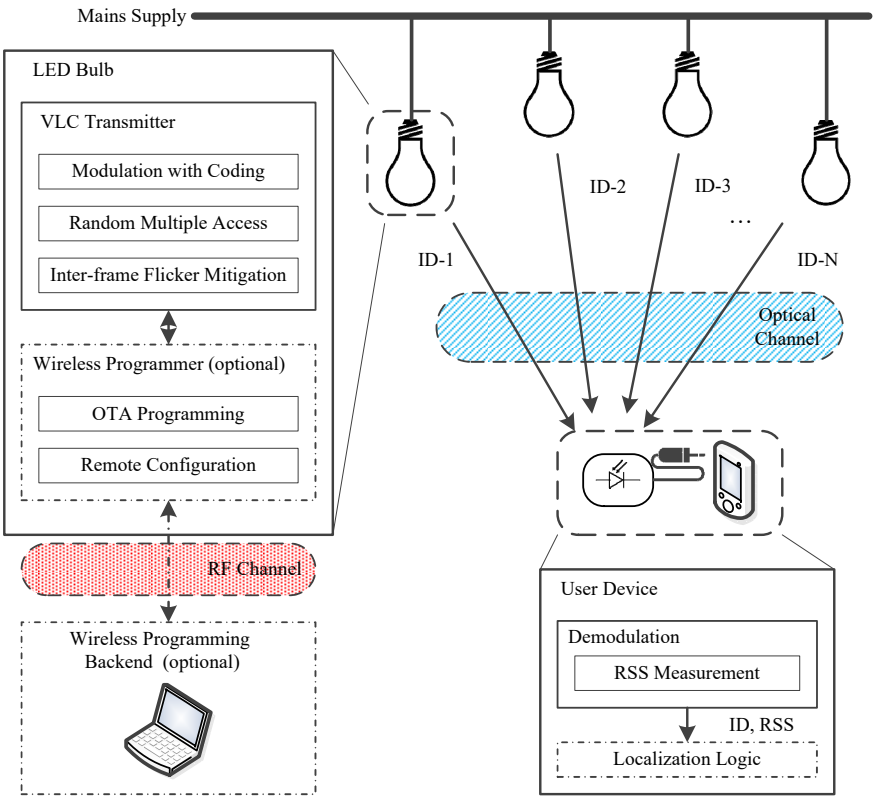

Figure 1: The Plugo System Architecture.

Each bulb exploits a microcontroller to implement all the communication logics as a firmware such as signal modulation and multiple access control. The beacon message is encoded by simple on-off keying (OOK) modulation with Manchester coding. Subject to one-way communication, the bulb could never know whether the sent beacon message has been correctly interpreted or not by the receiver. We adopt a BFSA-based random multiple access scheme in Plugo to prevent persistent collisions among these "blind" and uncoordinated light beacons. In addition, we have solved the induced inter-frame flicker problem.

To ease the system debugging such as the firmware update and parameter configuration, we come up with a standalone wireless programming system exploiting the RF channel. It consists of a backend and a number of wireless programmers residing in LED bulbs. Over-the-air (OTA) programming and remote configuration can be thus achieved. However, it should be highlighted that the RF links along with the wireless programming backend are not involved in beacon broadcasting. They only serve for debugging purpose.

3.1 Communication using OOK

3.1.1 Modulation and Coding

Many modulation schemes have been proposed for VLC, e.g., OOK, VPPM (Variable Pulse Position Modulation), and OFDM (Orthogonal Frequency Division Multiplexing). As for beacon broadcasting, a high data throughput is not necessary. We prefer a simple modulation scheme affordable in low-cost hardware components. To be specific, we choose the OOK modulation with Manchester coding which is also adopted by the IEEE 802.15.7 PHY I layer specification. It favors DC balance and easy clock recovery. While the binary frequency shift keying (BFSK) used by Epsilon [20] requires the FFT operation during the demodulation, OOK is even more lightweight as it can be demodulated on a low-cost microcontroller without DSP units. Constraints on the modulation frequency f_{mod} come from many factors such as the response time of LEDs, the perception bandwidth of photodiodes, the sampling frequency of the Analog-to-digital converter (ADC), etc. As for a proof-of-concept system implementation, we empirically choose $f_{mod} = 10\,\text{kHz}$ which is interpretable by a USB soundcard with a maximum sampling frequency of 48kHz.

3.1.2 Protocol Definition

Due to the limited modulation bandwidth of the low-cost hardware components, we do not chase a complete communication protocol with forward error correction (FEC) channel coding (e.g., Reed-Solomon and convolutional coding) and sophisticated MAC control mechanisms. Instead, we design a simple data frame structure that conforms to the beacon broadcasting application, as shown in Figure 2. It is composed of three sections, namely, start-of-frame (SOF), Data and end-of-frame (EOF). Figure 3 illustrates the frame composition using a sample of raw received VLC signals. SOF further contains a special frame delimiter (SFD) to indicate the start of a new frame and a Sync sequence for clock synchronization. The SFD here is indeed a 4-bit logic high symbol that never occurs in the normal Manchester coding data. The Sync sequence is 8-bit long with alternate high and low logic symbols that carry timing information. Similarly, the EOF contains a 4-bit logic low symbol ($\sim$SFD) to indicate the end of a frame. The data section consists of a 16-bit payload and a 4-bit checksum, which are both encoded by Manchester coding. The payload carries a unique identification code for each bulb. A 16-bit long code could easily cover a normal indoor environment with tens of thousands of lights. The checksum is generated by a simple XOR operation to verify the payload integrity. Once data corruption is detected at the receiver side, the message will be discarded. We do not perform any data retransmission under this circumstance, as the light beacon could not detect the potential transmission failure due to the lack of an uplink. Instead, the corrupted message could be recovered by subsequent observations.

3.2 Random Multiple Access

Random multiple access is the key difference between Plugo and many other systems that exploit fixed multiple access schemes such as FDMA and CDMA. To the best of our knowledge, it was only adopted by Epsilon [20] and Zhang's

SOF		Data		EOF
SFD	Sync	Payload	Checksum	~SFD
4 bits	8 bits	32 bits	8 bits	4 bits

Figure 2: Data Frame Structure

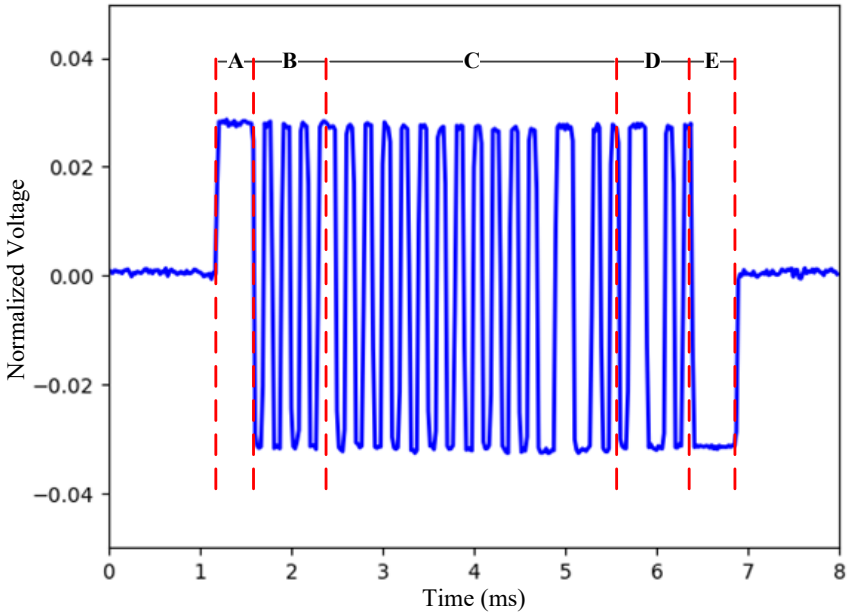

Figure 3: A typical raw received VLC signal fragment containing a full data frame. It is shown in a bipolar form as we adopt a USB sound card with AC coupling to acquire the analogue signal from the receiver front end. The signal amplitude is normalized within [-1.0, 1.0]. Notations A to E: A-SFD, B-Sync, C-Data Payload, D-Data Checksum, E-EOF.

work [21] in the previous literature. Epsilon proposed a frequency channel hopping scheme and showed its effectiveness through experiments. Zhang et al. introduced the BFSA scheme by simulation. It defines a transmission frame structure composed of a fixed number of time slots. Each light beacon selects randomly a time slot in the frame and transmits its beacon message within that slot. If any two adjacent lights select the same time slot or two overlapping time slots, there will be a transmission failure because of the conflicts. The corrupted messages could be recovered later as long as the beacons keep broadcasting.

We adopt the BFSA scheme to achieve random multiple access over the shared optical medium in a distributed VLC network that supports one-way communication. The success rate $P_{success}$ is an important metric to evaluate the system performance. It is defined in [21] as the probability of successful transmission from all transmitters inside a coverage vicinity to a given receiver. Supposing perfect synchronization among these transmitters, the theoretical value could be calculated by the following formula where N is the number of time slots per frame and n is the number of transmitters.

$$P_{success} = \frac{\left\langle {N \atop n} \right\rangle}{N^n}$$

As for an asynchronous system, starting points of the time slots from different lights are probably misaligned. The success rate will decrease when more collisions happen. $P_{success}$ increases with the number of time slots per frame N. Meanwhile, the communication bandwidth needed for each transmitter is also N times the original. We have to make a trade off between the success rate and communication bandwidth available on low-cost hardware components.

In the current implementation, the communication bandwidth is subject to the sampling frequency of the audio ADC of the soundcard. The average waiting period of the localization system is around $112ms$ when choosing $N = 20$ time slots for each transmission. It is also feasible to implement the signal demodulation on a microcontroller with on-chip ADCs whose sampling frequency can easily reach 1 MHz. One underlying prerequisite is that the adopted OOK modulation scheme is very lightweight to implement. It is expected to provide higher success rates along with shorter localization latency.

The LED bulb performs data transmission when the desired time slot comes and then goes to idle states. The Manchester coding data is DC balanced thus eliminating the intra-frame flicker of the bulb during the data transmission. However, how to mitigate the potential inter-frame flicker during the idle states remains a problem.

3.3 Inter-frame Flicker Mitigation

Flicker refers to the visible fluctuation of the light brightness [23]. It further comprises intra-frame flicker and inter-frame flicker. In this context, the intra-frame flicker has been eliminated by Manchester coding. Thus we focus on the mitigation of the inter-frame flicker. As suggested by the IEEE 802.15.7 standard [35], one can make the LED light transmit a dummy data message during the idle states to prevent flicker. The modulation frequency of the dummy message can either be in-band or out-of-band. In a particular case, the light can be driven by a suitable DC current free of modulation. The idea is straightforward — the overall brightness of the LED bulb will keep consistent as long as the DC

intensity during the idle time slots equals to the average intensity during the active time slots. The required DC current of each bulb varies. It is unlikely to tune it one by one.

As for the Plugo system, it is a bad way to modulate the dummy message by an in-band frequency because it can induce severe interference to other nodes who are broadcasting beacon messages. We prefer to modulate it by a high out-of-band frequency, e.g., 100 kHz in the current implementation, which can be removed easily by a low-pass filter on the receiver. The dummy message here is indeed repeated "01" symbols which provide an equal average intensity to the beacon message. Ideally, we may also choose a much lower frequency like 100 Hz which has to be filtered out by a high-pass filter. In this context, however, the modulated OOK signal will be distorted severely by the high-pass filter and become difficult to recover. This is due to the significant attenuation of the low-frequency components of the modulated square waves.

3.4 Localization using Gaussian Process Regression

As for the localization validation of the Plugo system, we adopt a fingerprinting-based localization algorithm which uses Gaussian process regression (GPR) [36] based on our previous work [22, 27]. To be specific, GPR is utilized to construct an intensity distribution model for the environment according to sparsely collected fingerprint samples. After that, a Bayes filter is used to do localization with respect to the built map. To conclude, the localization algorithm comprises the GPR-based environment modeling and Bayes filter-based localization.

3.4.1 GPR-based Environment Modelling

We consider a training set $\mathcal{D} = \{(\mathbf{x}_1, y_1), (\mathbf{x}_2, y_2), \ldots, (\mathbf{x}_n, y_n)\}$, where $\mathbf{x}_i$ denotes the input vector of a 2D position, y_i is the scalar observation of the received RSS for each light source. The observation is drawn from a noisy process $y_i = f(\mathbf{x}_i) + \epsilon$, where ϵ is an additive Gaussian noise with zero mean and known variance σ_n^2. For convenience in notations, the n inputs $\mathbf{x}_i$ are aggregated into a single matrix $\mathbf{X} \in \mathbb{R}^{n \times 2}$, and the observation values y_i into a column vector $\mathbf{y} \in \mathbb{R}^n$.

We use Gaussian process to predict the posterior distributions over functions f from the training set $\mathcal{D}$. The fundamental requirement of GPs is that the function values for different inputs are correlated. That is, the covariance between two function values $f(x_p)$ and $f(x_q)$ are dependant on the input values x_p and x_q. The covariance relationship could be represented by a kernel function $k(\mathbf{x}_p, \mathbf{x}_q)$. In practice, we normally choose a Gaussian kernel, a.k.a., the squared exponential kernel,

$$k(\mathbf{x}_p, \mathbf{x}_q) = \sigma_f^2 exp\left[-\frac{(\mathbf{x}_p - \mathbf{x}_q)^2}{2l^2}\right]$$

where σ_f^2 is the signal variance and l the length scale. These parameters specify how strongly the two points are correlated. The covariance function for the noisy observations $\{y_1, y_2, \ldots, y_n\}$ is,

$$cov(y_p, y_q) = k(\mathbf{x}_p, \mathbf{x}_q) + \sigma_n^2 \delta_{pq}$$

where σ_n^2 is the Gaussian noise and δ_{pq} is the Dirac function. As for the whole training set, we have

$$cov(\mathbf{y}) = \mathbf{K} + \sigma_n^2 \mathbf{I}$$

where $\mathbf{K} = [k(\mathbf{x}_p, \mathbf{x}_q)] \in \mathbb{R}^{n \times n}$ is the covariance matrix of the input values. The observation values in $\mathcal{D}$ are jointly Gaussian,

$$\mathbf{y} \sim N(\mathbf{0}, \mathbf{K} + \sigma_n^2 \mathbf{I})$$

. Given a new input $\mathbf{x}_*$, the posterior distribution over function values $f(\mathbf{x}_*)$ is Gaussian,

$$P\left(f(\mathbf{x}_*) \,|\, \mathbf{x}_*, \mathbf{X}, \mathbf{y}\right) = N\left(f(\mathbf{x}_*); \mu_{\mathbf{x}_*}, \sigma_{\mathbf{x}_*}^2\right)$$

where

$$\mu_{\mathbf{x}_*} = k_*^{\mathrm{T}} (\mathbf{K} + \sigma_n^2 \mathbf{I})^{-1} \mathbf{y}$$

and

$$\sigma_{\mathbf{x}_*}^2 = k(\mathbf{x}_*, \mathbf{x}_*) - k_*^{\mathrm{T}} (\mathbf{K} + \sigma_n^2 \mathbf{I})^{-1} k_*$$

. $k_* \in \mathbb{R}^n$ denotes the covariances between x_* and n training inputs $\mathbf{X}$.

Finally, we create a set of intensity distribution maps comprising the mean maps and variance maps for each light beacon. Figure 4 shows a sample of the generated maps for light #1. The mean map specifies the expected intensity distribution in the sampled area and the variance represents the confidence of the observation results.

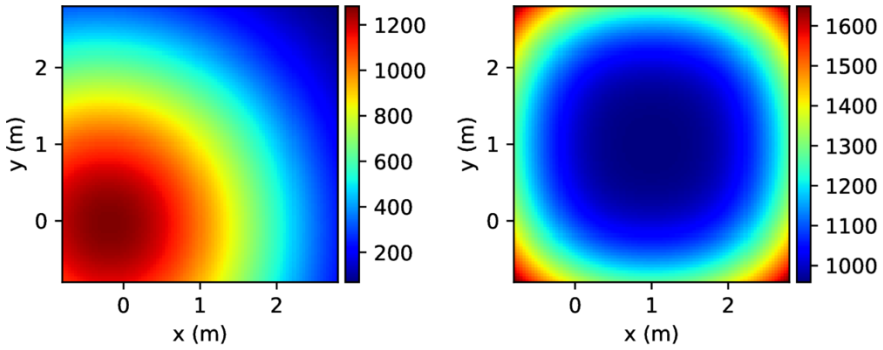

Figure 4: The intensity distribution map for light #1 generated by GPR. The left is the mean map and the right is the variance map.

3.4.2 Bayes Filter-based Localization

We use the Bayes filter to realize the localization with the built intensity distribution maps. The basic idea is to estimate the current position $\mathbf{x}_t$ on the basis of the history estimation results $\mathbf{x}_{0:t-1}$ and observations $\mathbf{y}_{0:t-1}$ which could be formulated as,

$$\begin{aligned} &P(\mathbf{x}_t \,|\, \mathbf{y}_{0:t}, \mathbf{u}_{0:t}) \propto P(\mathbf{y}_t \,|\, \mathbf{x}_t) \\ &\times \sum_{\mathbf{x}_{t-1}} P(\mathbf{x}_t \,|\, \mathbf{x}_{t-1}, \mathbf{u}_{t-1}) P(\mathbf{x}_{t-1} \,|\, \mathbf{y}_{0:t-1}, \mathbf{u}_{0:t-1}) \end{aligned}$$

where, $\mathbf{u}_{0:t}$ is the control input, $P(\mathbf{y}_t \,|\, \mathbf{x}_t)$ is the observation model from GPR, $P(\mathbf{x}_t \,|\, \mathbf{x}_{t-1}, \mathbf{u}_{t-1})$ is the motion model, and $P(\mathbf{x}_{t-1} \,|\, \mathbf{y}_{0:t-1}, \mathbf{u}_{0:t-1})$ is the previous estimation state. In the current implementation, we do not involve any motion measurement, e.g., using an IMU. The motion model respects a zero-mean Gaussian distribution supposing that the transient position is static and tends to move in any direction described by σ^2. We initialize the location prior using an uniform distribution. The localization result could be solved by the maximum-a-posterior (MAP) estimation illustrated as,

$$\hat{\mathbf{x}}_t = \underset{\mathbf{x}_t}{\operatorname{argmax}} \{P(\mathbf{x}_t \,|\, \mathbf{y}_{0:t}, \mathbf{u}_{0:t})\}$$

4 Implementation Details

4.1 VLC-compatible LED Bulbs

Figure 5: The fully assembled LED bulb.

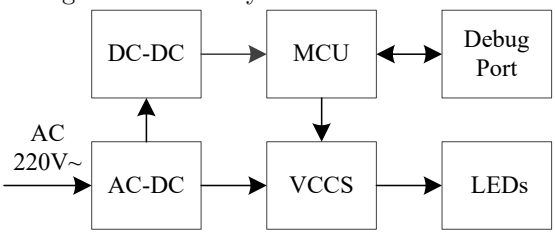

Figure 6: Schematic diagram of the LED bulb driver circuitry

The VLC functionality is not yet available on off-the-shelf LED lights. As shown in Figure 5, we aim at a compact design of the LED bulb which is easy to use in a plug-and-go fashion. The bulb is designed with a standard E27 screw base so that it can be easily installed to a lamp socket. The schematic of the LED driver is shown in Figure 6. It consists of an AC-DC power supply, a DC-DC buck converter, a voltage-controlled current source (VCCS), a low-cost microcontroller (MCU), a debug connector, and a LED plate. The AC-DC power module provides an output of 12 V with a maximum power of 4.5 W.

We choose a 3 W LED plate, considering the power tolerance. The DC-DC converter steps down 12 V to 5 V to power other circuits. The LED current is adjusted by the VCCS under the control of the microcontroller. The signal modulation, coding, and the random multiple access control are all implemented in the microcontroller as a firmware. With the aid of a wireless programmer, the firmware can be updated over the air on demand. We build the bulbs on the top of a set of off-the-shelf LED bulb components, as shown in Figure 7. The aluminum made bulb case is good for heat dissipation. Moreover, there is enough room inside the case to hold a small driver circuitry.

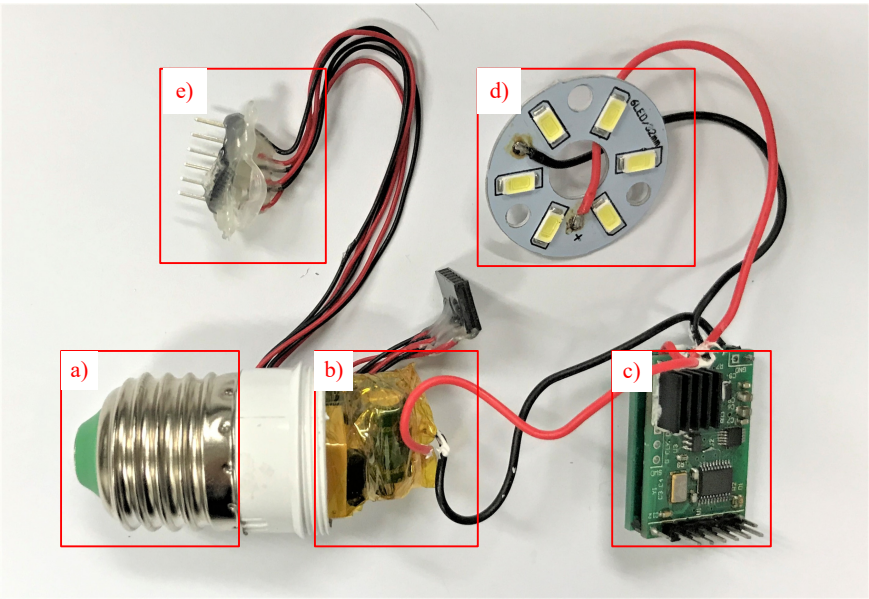

Figure 7: The primary components of LED bulbs. a) a standard E27 screw base, b) an off-the-shelf AC-DC power supply, c) the VLC control board integrating a DC-DC converter and a microcontroller, d) a LED plate, and e) a debugging connector. The bulb case and shade are omitted for simplicity.

4.2 Photodiode Receiver

The schematic of the designed receiver circuitry is shown in Figure 8. It is composed of a PIN photodiode (PD), a trans-impedance amplifier (TIA) with DC bias correction, a low-pass filter (LPF), and a small lithium battery. We connect the receiver to a USB soundcard via an audio jack. The signal acquisition and demodulation are implemented on the computer with the *python-alsaaudio* [1] library. The lithium battery can be recharged via a micro USB connector. Figure 9 shows the assembled circuitry.

The ambient interference comes from sunlight along with the fluorescent or incandescent lights. It includes a large DC bias, some strong low-frequency components (100 or 120 Hz), and high-frequency harmonics. Besides, the dummy message broadcasting in our system also introduces a significant high-frequency

[1] `https://larsimmisch.github.io/pyalsaaudio/`

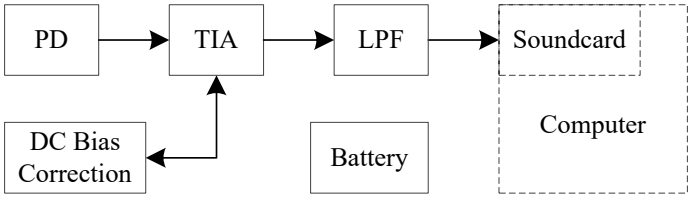

Figure 8: Schematic diagram of the photodiode receiver circuitry

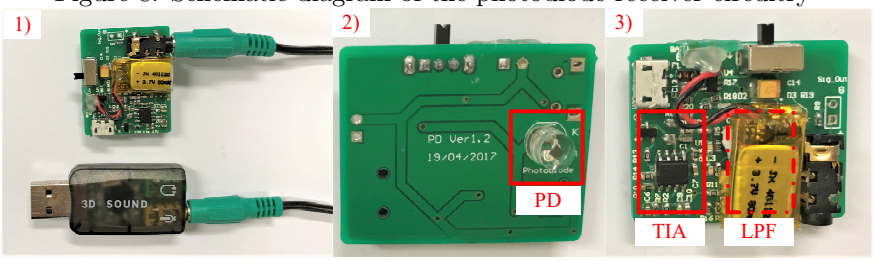

Figure 9: (1) The receiver circuitry connected with a USB sound card via the audio jack; (2) Top view of the PCB showing the photodiode (highlighted in the red rectangle); (3) Bottom view of the PCB showing the TIA and LPF (covered by the lithium battery).

component. A large DC bias may cause saturation of the receiver circuitry. To circumvent this situation, we involve an error integrator to TIA so as to correct the induced DC bias. The output signal bias is stabilized to a fixed value in spite of the ambient interference. We adopt a fourth-order Butterworth low-pass filter to remove the significant high-frequency interference from the dummy broadcasting. We do not take care of the low-frequency interference in the current implementation.

4.3 Wireless Programming System

The wireless programming system is designed to fulfill two primary functions—1) over-the-air (OTA) programming and 2) remote configuration. The motivation arises from the needs of system debugging in a large-scale environment, e.g., with tens or hundreds of VLC-compatible LED bulbs. During the debug session, we may modify the firmware of the bulbs or alter configuration parameters from time to time. It would turn to be a nightmare if we have to unscrew each bulb and flash a firmware image piece by piece. To circumvent this situation, a wireless programming system comes to play. It consists of a master node (Figure 10-1) connected with a computer as the backend and a number of slave nodes (Figure 10-2) attached to the LED bulbs. They are assembled on the basis of a shared hardware design albeit running different versions of firmware. We build several hardware prototypes using off-the-shelf components including a microcontroller board with a USB interface and a low-cost 2.4G RF communication module. To cover a broader area, the RF module in the master node bears a larger transmission power considering that the data traffic occurs mainly in the downlink.

The master node is in charge of each communication session. It could talk

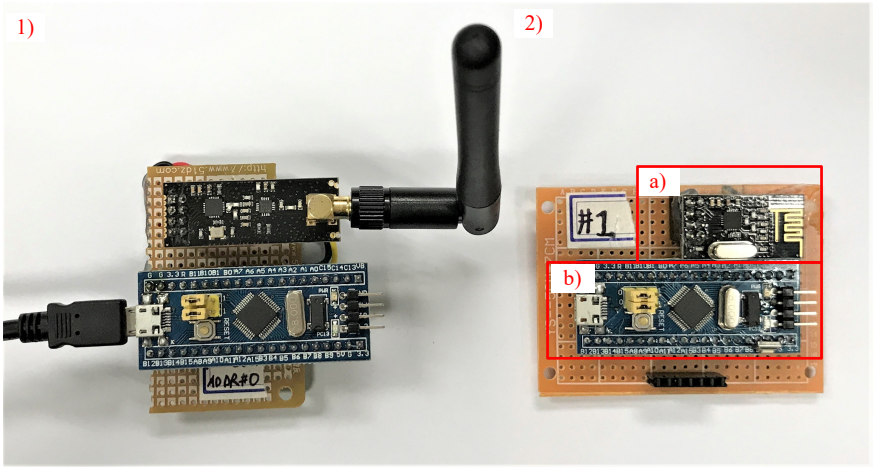

Figure 10: The wireless programming system prototype. (1): The master node with a high-gain antenna; (2): The slave node consisting of a microcontroller boad a) and a RF module b).

to any slave nodes by assigning a specific destination address so as to initiate a firmware update or parameter configuration. All the control logics are implemented as a firmware inside the microcontroller. The master node could be configured by the computer via the USB interface using a set of customized "AT" commands. As for the OTA programming, the computer specifies the destination address along with other necessary parameters for RF communication (e.g., channel frequency) and sends the firmware image to be flashed to the master node through USB. The firmware file will be packaged and then dispatched to the designated slave node. The slave will recover the firmware image and check its integrity. If the received file is valid, the slave node will embark on the firmware downloading using in-system-programming (ISP) via the UART communication with the target bulb. Besides, we have implemented a virtual serial communication protocol which is transparent to users on top of RF links. As a consequence, remote configuration of LED bulbs is feasible.

5 System Evaluation

In this section, we evaluate Plugo first with a small customized testbed through field experiments, and then simulations for large-scale scenarios. As for the field experiments, we focus on the evaluation of basic beacon broadcasting capability of Plugo along with its localization performance in real applications. We implement a fingerprinting-based localization algorithm and present a preliminary localization result demonstrating the localization accuracy, consistency, responsiveness and robustness. To further explore the system scalability to large-scale scenarios, we conduct simulations in a floor-size environment evaluating the beacon broadcasting along with the localization feasibility.

We set up an indoor localization testbed in our lab with four customized LED bulbs, as shown in Figure 11. Four bulbs are installed at the corners of a $3m \times 3m$ square testbed with a height of $2.37m$ over the ground. In the adopted

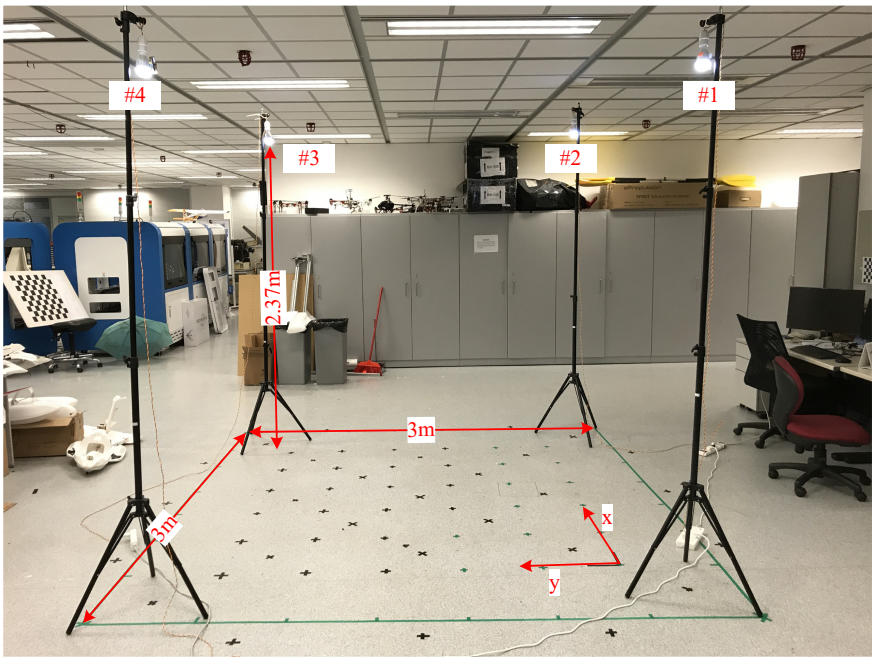

Figure 11: Testbed with four LED bulbs: light#1, light#2, light#3 and light#4. The x-axis and y-axis are labelled with single-end arrows.

localization algorithm, we use GPR to build a fine-grained light intensity map upon sparse fingerprint samples. We create a 2D grid with 6×6 points spaced at $0.4m$ as the training samples for GPR in the central area, as shown in Figure 12. Then we evenly select 25 extra positions for evaluation covering both the central and border area. We locate these points with an accuracy around $2cm$ with the aid of a commodity laser range finder.

5.1 Beacon Broadcasting

Figure 13 shows a sample of raw VLC signals received simultaneously from four LED bulbs. It is clear that beacon messages are randomly distributed in the time domain. In most cases, they are separated neatly and can be successfully recovered. When collisions occur, as shown in Figure 13-b), messages involved will be corrupted. However, we can safely retrieve them by continuous observations later on. Figure 13-a) shows a special case. The received message is decodable and checked to be correct by the received checksum. However, there exists a noticeable fluctuation in the signal waveform which is indeed corrupted by others. The RSS measurement is distorted in this situation and may further degrade the localization performance. As a result, we would prefer to discard it.

We measure the success rate $P_{success}$ of the BFSA-based multiple access scheme and compare it with the theoretical result in Figure 14. The measured values are inferior to the theoretical ones due to the lack of synchronization among the lights. $P_{success}$ increases with the number of time slots per frame N. In our implementation, we use a USB soundcard as the ADC on the receiver

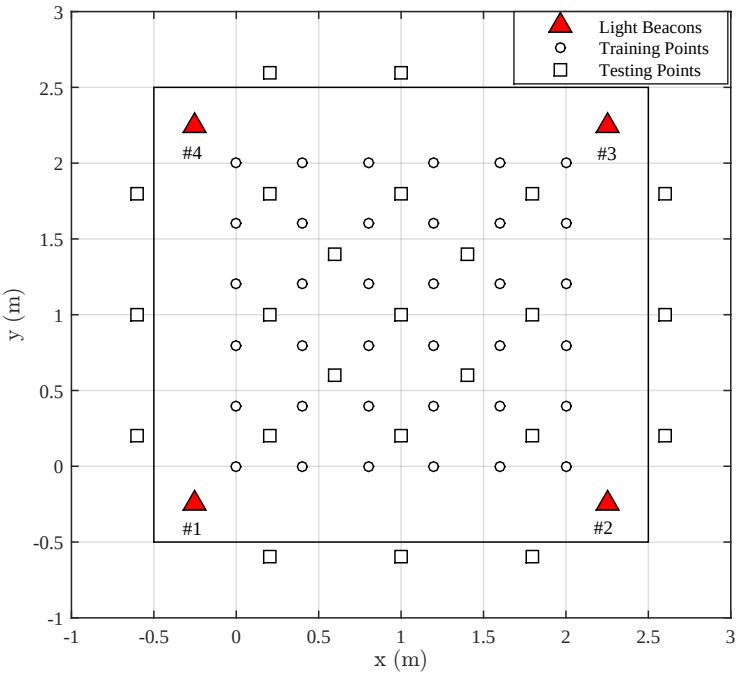

Figure 12: Testbed floor plan illustrating the training and testing points.

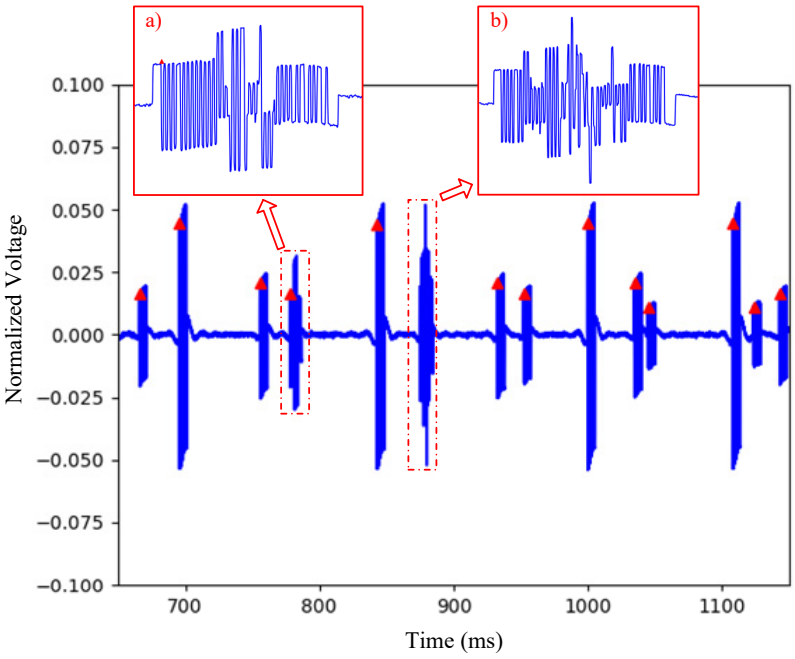

Figure 13: A fragment of raw VLC signals received from four LED bulbs. The decodable messages are marked by red triangles. a) and b) show magnified views of typical corrupted signals.

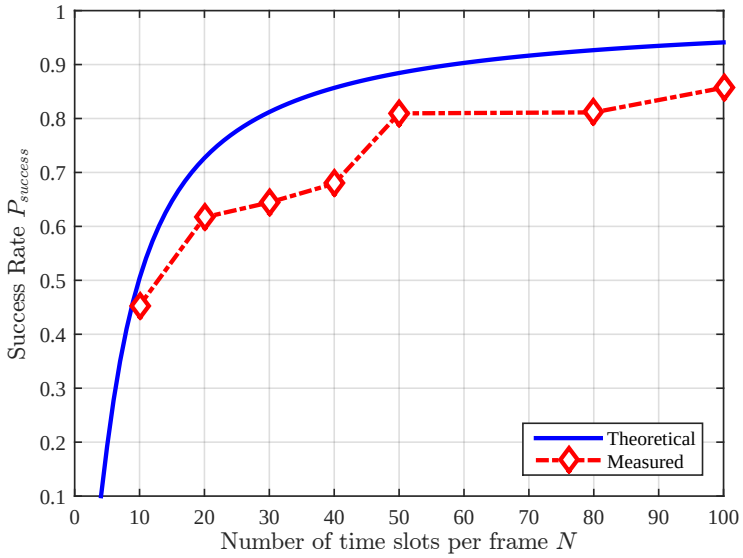

Figure 14: Success rate versus number of time slots per frame.

side with a maximum sampling rate of 48 kHz. To grant reliable signal recovery, the OOK modulation frequency is set to 10 kHz. It takes around 5.6 ms to transmit a full data packet. So as to provide an acceptable localization latency, we empirically choose $N = 20$ for each transmission frame.

5.2 Localization with Plugo

During the localization experiment, we turn on the four bulbs and keep other lights off. This is because the maximum power (3W) of the LED bulbs is much lower than the normal power rating of other fluorescent lights. The low-frequency components with high energy from these lights will cause the saturation of the receiver circuitry. However, we claim that this will not be a problem if we use higher-power LED lights as we can choose a smaller amplifying gain to prevent the saturation.

We collect fingerprint samples at 36 positions and build the intensity distribution maps for all the light beacons. The map for light #1 is shown in Figure 4. We first conduct the experiment at 25 static positions which are illustrated in Figure 12. The estimated positions along with the groundtruth are plotted in Figure 15. The maximum localization errors occur near the testbed borders. This is because we only collect fingerprint samples in the central area of the testbed. The generated light intensity map does not fit well the intensity distribution in the border area. Figure 16 plots the empirical CDF of the position errors with the solid curve. The average error is $0.14m$ and the 90-percentile error is $0.33m$. To evaluate the robustness to lights failure, we deliberately switch off light #4 and redo the experiment. The position error CDF is shown by the dashed line in Figure 16. The localization accuracy is slightly degraded. But we still achieve an average error of $0.17m$ and a 90-percentile error of $0.50m$. It shows that the localization system built upon Plugo is robust to the absence of lights to some extent.

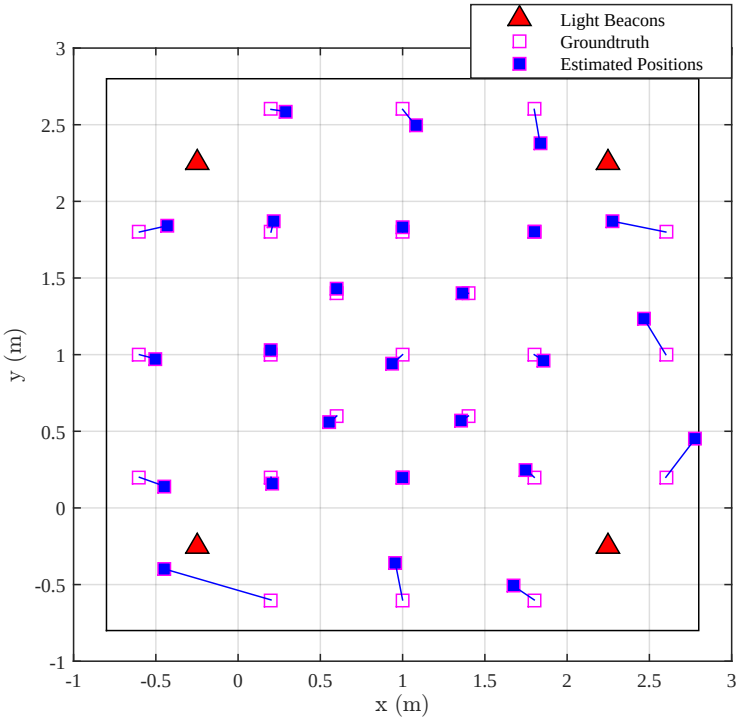

Figure 15: Localization results at 25 static positions.

We also evaluate the consistency of the localization results. Specifically, we fix the VLC receiver on the center of the testbed and record the estimated positions continuously for 300s, as shown in Figure 17. The average error is $0.046m$ and the standard deviation is $0.01m$. The error plot appears to be discrete. This is because of the discretization of the intensity distribution maps with a resolution of $0.04m$. It is reasonable that the average error is comparable to the map resolution. The error variation at the static position is relatively small which demonstrates sound system consistency. To demonstrate a real-time use case, we move the receiver on the ground along a fixed trajectory comprising two closed rectangles, as shown in Figure 18. The estimated trajectory includes two close-loops similar to the groundtruth. We notice large errors around $0.4m$ near the testbed borders and small errors in the central area. This reveals the limitation of the adopted localization algorithm.

5.3 Simulation of Large-scale Scenarios

Since the hardware-based testbed covers a limited scope of $3m \times 3m$ and involves only four LED bulbs, it prevents us from exploring the system scalability to large-scale scenarios. To circumvent this situation, we perform simulations of the beacon broadcasting along with localization in a floor-size indoor environment with tens of LED bulbs.

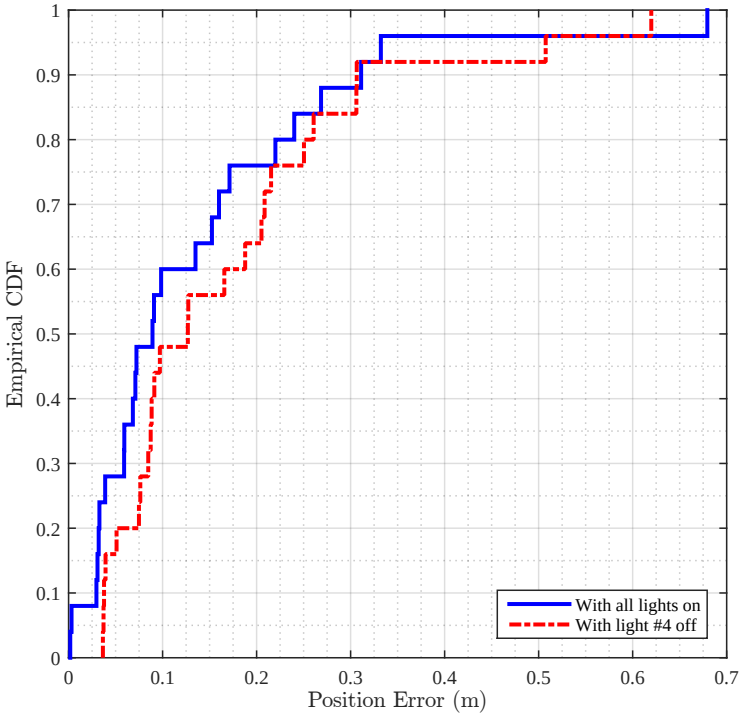

Figure 16: Position estimation error CDF when four lights are turned on (with solid lines) and one light off (with dashed lines).

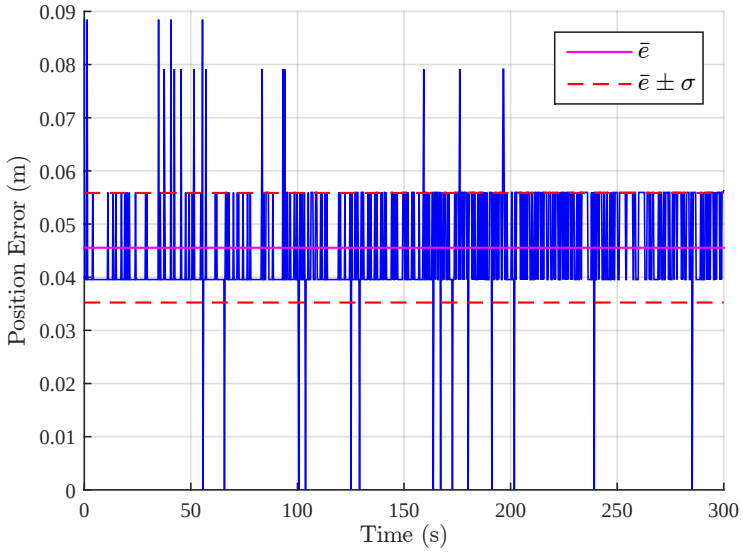

Figure 17: Localization error at $(1.0, 1.0)$ with respect to time.

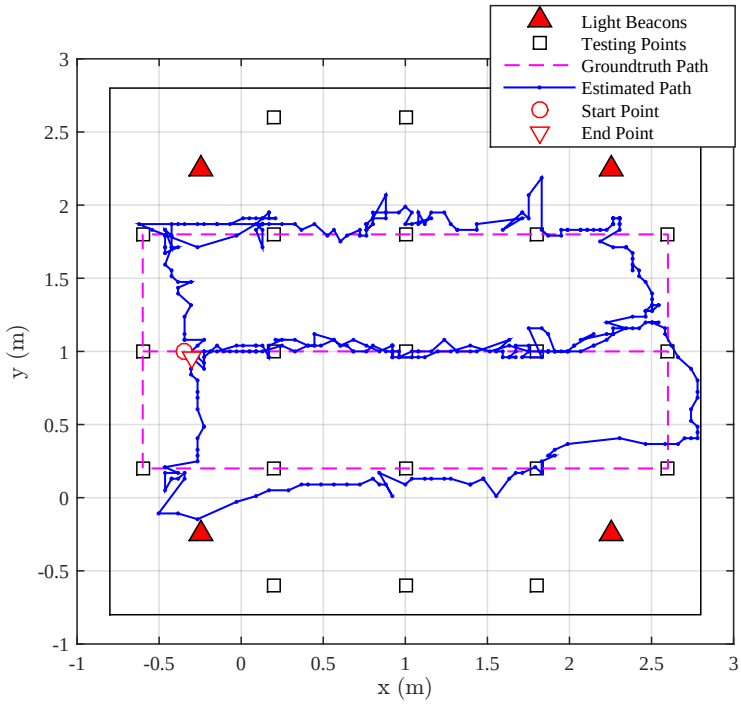

Figure 18: Continuous localization results along a fixed trajectory.

5.3.1 Beacon Broadcasting

The simulation space is of size $30m \times 30m \times 2.5m$. We place 81 LED bulbs evenly on the ceiling with a separation of $3m$, and put the receiver on the ground. The vertical distance is fixed to $h = 2.5m$ between the receiver and each light. We create a 40×40 grid uniformly distributed on the ground and evaluate the beacon broadcasting performance on each grid point.

In Section V.A, we adopt the success rate $P_{success}$ as the evaluation metric of beacon broadcasting in the field experiment, where we take all the four lights into consideration and measure the success rate of recovering all the data packets from these lights. However, in the large-scale simulation situation, it is inappropriate to involve all the lights to localization. Lights that are out of the FOV or far away from the receiver contribute little to the improvement of localization performance. Empirically, we intend to select the top four strongest signals for localization. This is because the strongest signal normally comes from a nearer LED light at a smaller incidence angle compared to others. It will induce fewer uncertainties in RSS measurement.

As for conventional geometry-based localization methods, the minimum number of beacons is three for 2D localization and four for 3D cases. From the robot state estimation perspective, however, we believe that this requirement can be relaxed. That is, any number of effective measurements of the surrounding environment could probably help improve the location estimation. To this end, we slightly modify the definition of success rate $P_{success}$ as the total number of successfully received messages over the number of sent messages from the top

four strongest signal sources.

In a nutshell, we will measure the success rate at each evaluation point on the ground considering only the top four strongest signals perceived by the receiver. If the success rates are acceptable in the whole evaluation area, we may safely consider that the beacon broadcasting performance of Plugo is well scalable to large-scale scenarios.

The radiation pattern of most LED bulbs could be accurately characterized by the Lambertian model [20]. Here we adopt a simplified first-order Lambertian model formulated by

$$H(0) = \begin{cases} C\,\frac{cos\,\psi cos\,\phi}{d^2} & (\phi \leq \Phi_c) \\ 0 & \text{otherwise} \end{cases}$$

where $H(0)$ is the DC channel gain at the receiver side, C is a constant which accounts for the LED radiation power and the receiver amplifying gain, ψ and ϕ are respectively the irradiation angle of LED bulbs and incidence angle of the photodiode receiver, d is the LOS distance between the bulb and receiver, and Φ_c is the photodiode FOV (70° in our case). The constant C is calibrated once for good.

To further simplify the simulation scenario, we assume the photodiode receiver always faces upwards the ceiling and all the bulbs face downwards the ground. Accordingly, we have

$$\psi = \phi = cos^{-1}\frac{h}{d} \quad (\phi \leq \Phi_c)$$

and

$$H(0) = C\,\frac{h^2}{d^4} \quad (\phi \leq \Phi_c)$$

. To this end, the channel gains at different receiving locations could be easily calculated for each LED bulb.

We generate an artificial VLC signal sequence for each LED bulb embedding its unique identification code using OOK modulation with Manchester coding along with the BFSA-based multiple access control. The data frame structure is the same as that used in a real LED bulb. To be specific, we choose $N = 20$ time slots per transmission and conduct 20 times of beacon transmissions. As a result, we have 400 time slots in total for each VLC signal sequence. The received VLC signal at each evaluation location is a linear combination of VLC signals emitted by all the lights within the photodiode FOV weighted by the corresponding DC channel gains. Finally, we feed the generated signals to the decoding procedure used by field experiments and calculate the success rates.

Figure 19 plots the histogram of the success rates evaluated at 1600 positions that are evenly selected on the ground. Most success rates center on the median value of 0.85. The "tall and thin" shape of the histogram implies reliable beacon broadcasting performance in the large-scale simulation environment. We notice that the average success rate is much higher than that measured in the field experiment which also adopts $N = 20$ time slots per transmission. This is because the time slots for different LED bulbs is perfectly aligned in the simulation cases. Collisions are thus avoided due to the partial overlap of time slots that are frequently encountered in real applications. In addition, we simulate the noise in beacon broadcasting using an additive white Gaussian noise with a

small amplitude. In the real scenario, however, the noises may be much severe thus degrading the success rate. Then we set $N = 50$ and redo the simulation with the results shown in Figure 20. The histogram is shifted to the right with a higher median value around 0.93 along with a much smaller spread. This reveals that the beacon broadcasting performance improves with the number of time slots assigned to each transmission.

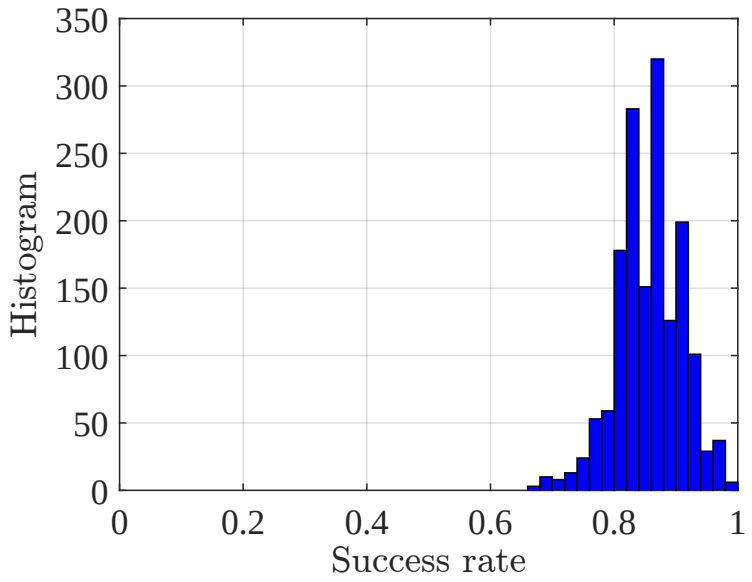

Figure 19: Histogram of the success rates at 1600 positions with N=20.

5.3.2 Localization

We set up a simulation environment sketching the second floor of the CYT building in HKUST, as shown in Figure 21, which consists of some representative indoor scenarios such as corridors, offices and laboratories. The total coverage area is of size $55m \times 40m$. Specifically, we evaluate the large-scale localization performance in the circular corridor along with the laboratory. We place 83 modulated lights on the ceiling with a fixed height of $2.5m$ to the receiver plane. Besides, the receiver is assumed to face upwards and have an FOV of $70°$.

We implement a fingerprinting-based localization method similar to that of the field experiments. First, we build the intensity distribution maps for each light and show several of them in Figure 22. During the simulation scenario, an individual sets out from the starting point on the upper-left corner, walks anticlockwise along the corridor, goes through the lab and returns back finally. The walking trace covers a majority part of the circular corridor and the lab.

The simulation results are illustrated in Figure 21. The estimated positions are shown by the plus signs. Besides, the color variations on the plot show the corresponding estimation uncertainties. Intuitively, the estimated path matches the ground truth quite well. In addition, the empirical CDF of the position estimation errors is plotted in Figure 23. The average and 90-percentile errors are around $0.40m$ and $0.78m$ respectively, which are acceptable for the indi-

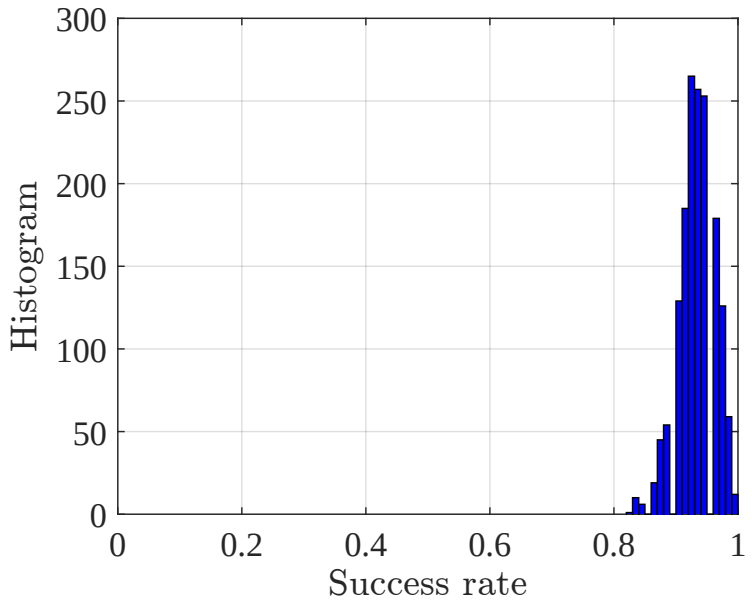

Figure 20: Histogram of the success rates at 1600 positions with N=50.

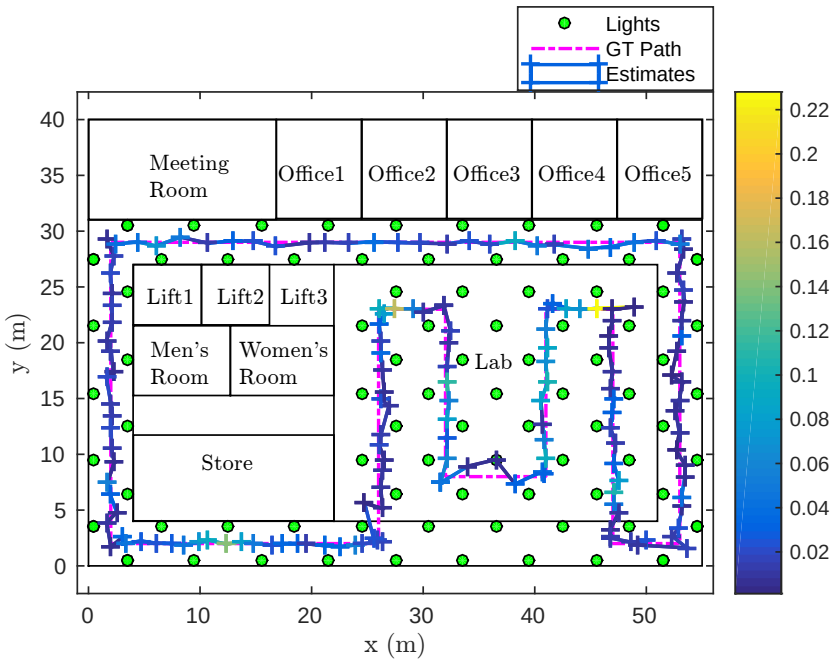

Figure 21: Illustration of the simulation environment: the ground truth testing path is plotted by the solid-dashed line, and the estimated path is marked by the plus signs colored by the estimation uncertainties.

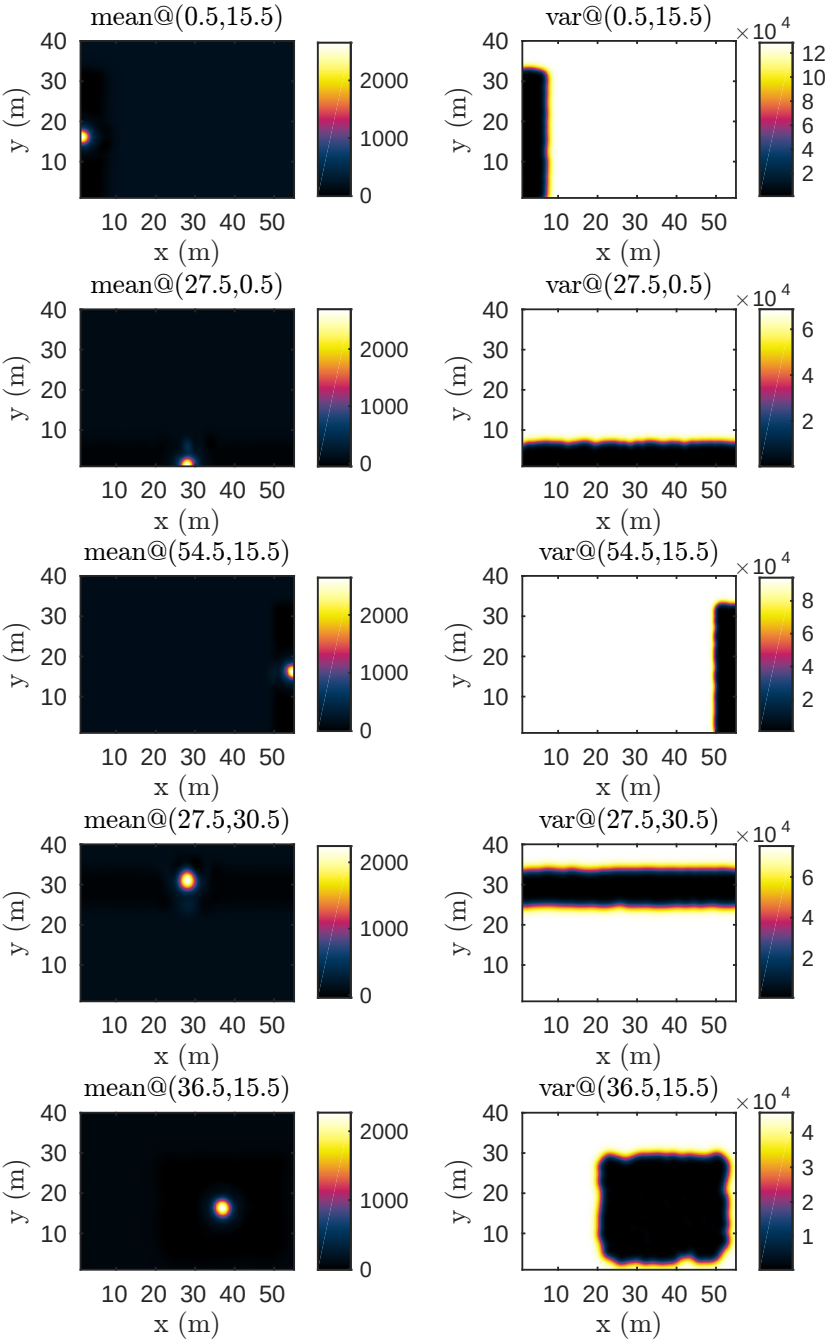

Figure 22: Intensity distribution maps generated by GPR for 5 representative lights which are located in the circular corridor and the lab at $(0.5, 15.5)$,$(27.5, 0.5)$,$(54.5, 15.5)$,$(27.5, 30.5)$,$(36.5, 15.5)$.

vidual way-finding. The localization accuracy is inferior to that of the field experiments, mainly due to the coarse granularity of the built maps. As the map size grows quadratically when the granularity decreases, we choose $0.15m$ in the simulation to make the map generation and fingerprints matching process tractable. It is possible to improve the localization accuracy yet at the cost of finer maps and longer processing time, which may violate the responsiveness in real-time applications.

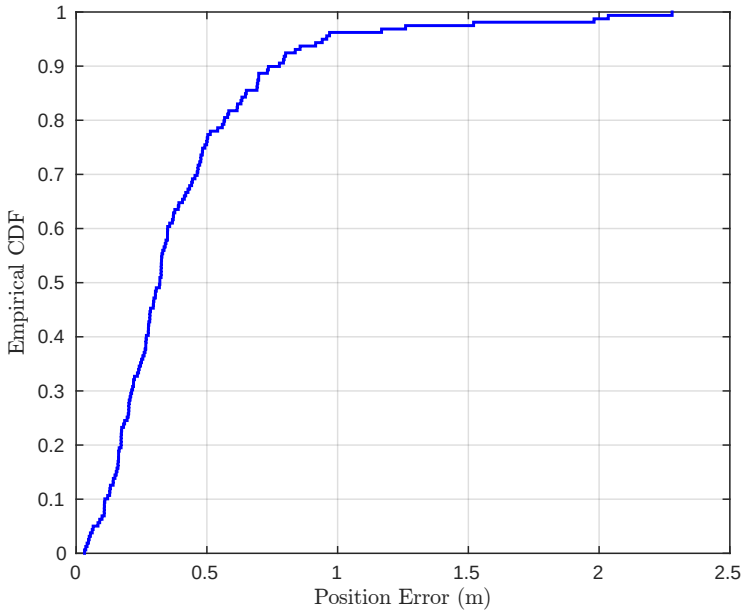

Figure 23: The empirical CDF of position errors in the simulation.

5.4 Discussion

According to the key technical criteria identified in Section II.B for the expected large-scale indoor localization technologies, we briefly discuss the system performance of Plugo in beacon broadcasting and localization.

Accuracy & Precision: Through the fingerprinting-based localization algorithm, we demonstrated the feasibility of accurate localization using Plugo. We have achieved an average accuracy of $0.14m$ and a 90-percentile accuracy of $0.33m$. In the literature, the 90-percentile accuracy is normally adopted as the precision evaluation metric.

Responsiveness: We demonstrated a real-time application of the prototyping localization system by tracking a moving receiver along close-loops on the ground with an update rate around 9 Hz. The estimated trajectory showed sound geometry consistency.

Scalability: In Section II, we analyzed qualitatively the system scalability. Moreover, we demonstrated the system scalability in beacon broadcasting to large-scale scenarios, and showed the feasibility of VLC-based localization in a floor-size environment by simulation.

Robustness: We considered a special case of light failure by switching off one of the four lights. The localization accuracy is slightly degraded but still acceptable. The result has revealed, to some extent, the system robustness.

Other Criteria: The remainder of the aforementioned criteria are characterized by "lightweight", "low-cost", and "ubiquitous". We emphasize that, according to previous discussions, they are inherently fulfilled by VLC-based localization systems using photodiode receivers.

6 CONCLUSIONS

In this paper, we presented the design, implementation, and evaluation of Plugo, a dedicated VLC system towards large-scale localization. It was built upon a number of customized commodity LED bulbs and a photodiode receiver. Specially, the bulbs are with compact design favoring the plug-and-go deployment. We conducted an in-depth discussion of the design constraints along with considerations for a photodiode-based VLC system towards large-scale localization. Accordingly, we identified three underlying enablers: 1) distributed architecture, 2) one-way communication, and 3) random multiple access. A BFSA-based random multiple access scheme was implemented with practical issues taken into account. Experiment results showed that Plugo was able to achieve reliable beacon broadcasting over the shared optical medium. In addition, we demonstrated its scalability to large-scale scenarios through simulation. Finally, a preliminary localization result is demonstrated using Plugo in a $3m \times 3m$ square testbed showing an average accuracy of $0.14m$ and a 90-percentile accuracy of $0.33m$, which has been greatly improved comparing with the state-of-the-art.

References

[1] Y.-S. Kuo, P. Pannuto, K.-J. Hsiao, and P. Dutta, "Luxapose: Indoor positioning with mobile phones and visible light," in *Proceedings of the 20th annual international conference on Mobile computing and networking*. ACM, 2014, pp. 447–458.

[2] J. Armstrong, Y. Sekercioglu, and A. Neild, "Visible light positioning: a roadmap for international standardization," *IEEE Communications Magazine*, vol. 51, no. 12, pp. 68–73, 2013.

[3] J. Aleksandar, "A high accuracy indoor positioning system based on visible light communication," https://www.qualcomm.com/media/documents/files/lumicast-whitepaper.pdf, accessed June 9, 2017.

[4] MarketsandMarkets, "Indoor location market by component (technology, software tools, and services), application, end user (transportation, hospitality, entertainment, shopping, and public buildings), and region - global forecast to 2021," http://www.marketsandmarkets.com/Market-Reports/indoor-positioning-navigation-ipin-market-989.html, accessed June 9, 2017.

[5] H. Liu, H. Darabi, P. Banerjee, and J. Liu, "Survey of wireless indoor positioning techniques and systems," *IEEE Transactions on Systems, Man,*

and Cybernetics, Part C (Applications and Reviews), vol. 37, no. 6, pp. 1067–1080, 2007.

[6] C. Cadena, L. Carlone, H. Carrillo, Y. Latif, D. Scaramuzza, J. Neira, I. Reid, and J. Leonard, "Past, Present, and Future of Simultaneous Localization and Mapping: Toward the Robust-Perception Age," *IEEE Transactions on Robotics*, vol. 32, no. 6, pp. 1309–1332, 2016. [Online]. Available: http://ieeexplore.ieee.org/document/7747236/

[7] T. Botterill, S. Mills, and R. Green, "Correcting scale drift by object recognition in single-camera SLAM," *IEEE Transactions on Cybernetics*, vol. 43, no. 6, pp. 1767–1780, 2013.

[8] L. Li, Y.-H. Liu, K. Wang, and M. Fang, "Estimating Position of Mobile Robots From Omnidirectional Vision Using an Adaptive Algorithm." *IEEE Transactions on Cybernetics*, vol. 45, no. 8, pp. 1–14, 2014. [Online]. Available: http://www.ncbi.nlm.nih.gov/pubmed/25265622

[9] C. Zhong, S. Liu, Q. Lu, B. Zhang, and S. X. Yang, "An efficient fine-to-coarse wayfinding strategy for robot navigation in regionalized environments," *IEEE transactions on cybernetics*, vol. 46, no. 12, pp. 3157–3170, 2016.

[10] A. Zhu and S. X. Yang, "Neurofuzzy-based approach to mobile robot navigation in unknown environments," *IEEE Transactions on Systems, Man, and Cybernetics, Part C (Applications and Reviews)*, vol. 37, no. 4, pp. 610–621, 2007.

[11] S. X. Yang and C. Luo, "A neural network approach to complete coverage path planning," *IEEE Transactions on Systems, Man, and Cybernetics, Part B (Cybernetics)*, vol. 34, no. 1, pp. 718–724, 2004.

[12] T.-H. Do and M. Yoo, "An in-depth survey of visible light communication based positioning systems," *Sensors*, vol. 16, no. 5, p. 678, 2016.

[13] J. Huang, D. Millman, M. Quigley, D. Stavens, S. Thrun, and A. Aggarwal, "Efficient, generalized indoor wifi graphslam," in *Robotics and Automation (ICRA), 2011 IEEE International Conference on*. IEEE, 2011, pp. 1038–1043.

[14] Y. Sun, M. Liu, and M. Q.-H. Meng, "Wifi signal strength-based robot indoor localization," in *Information and Automation (ICIA), 2014 IEEE International Conference on*. IEEE, 2014, pp. 250–256.

[15] T. Sathyan, D. Humphrey, and M. Hedley, "WASP: A system and algorithms for accurate radio localization using low-cost hardware," *IEEE Transactions on Systems, Man and Cybernetics Part C: Applications and Reviews*, vol. 41, no. 2, pp. 211–222, 2011.

[16] Y. Kim, Y. Chon, and H. Cha, "Smartphone-based collaborative and autonomous radio fingerprinting," *IEEE Transactions on Systems, Man and Cybernetics Part C: Applications and Reviews*, vol. 42, no. 1, pp. 112–122, 2012.

[17] H. Shin, Y. Chon, and H. Cha, "Unsupervised construction of an indoor floor plan using a smartphone," *IEEE Transactions on Systems, Man and Cybernetics Part C: Applications and Reviews*, vol. 42, no. 6, pp. 889–898, 2012.

[18] Z. Wu, Q. Xu, J. Li, C. Fu, Q. Xuan, and Y. Xiang, "Passive Indoor Localization Based on CSI and Naive Bayes Classification," *IEEE Transactions on Systems, Man and Cybernetics: Systems*, pp. 1–12, 2017.

[19] Z. Yang, Z. Wang, J. Zhang, C. Huang, and Q. Zhang, "Wearables can afford: Light-weight indoor positioning with visible light," in *Proceedings of the 13th Annual International Conference on Mobile Systems, Applications, and Services*. ACM, 2015, pp. 317–330.

[20] L. Li, P. Hu, C. Peng, G. Shen, and F. Zhao, "Epsilon: A visible light based positioning system." in *NSDI*, 2014, pp. 331–343.

[21] W. Zhang, M. S. Chowdhury, and M. Kavehrad, "Asynchronous indoor positioning system based on visible light communications," *Optical Engineering*, vol. 53, no. 4, pp. 045 105–045 105, 2014.

[22] K. Qiu, F. Zhang, and M. Liu, "Let the light guide us: Vlc-based localization," *IEEE Robotics & Automation Magazine*, vol. 23, no. 4, pp. 174–183, 2016.

[23] S. Rajagopal, R. D. Roberts, and S.-K. Lim, "Ieee 802.15. 7 visible light communication: modulation schemes and dimming support," *IEEE Communications Magazine*, vol. 50, no. 3, 2012.

[24] F. Zhang, K. Qiu, and M. Liu, "Asynchronous blind signal decomposition using tiny-length code for visible light communication-based indoor localization," in *Robotics and Automation (ICRA), 2015 IEEE International Conference on*. IEEE, 2015, pp. 2800–2805.

[25] Y.-A. Chen, Y.-T. Chang, Y.-C. Tseng, and W.-T. Chen, "A framework for simultaneous message broadcasting using cdma-based visible light communications," *IEEE Sensors Journal*, vol. 15, no. 12, pp. 6819–6827, 2015.

[26] D. Karunatilaka, F. Zafar, V. Kalavally, and R. Parthiban, "Led based indoor visible light communications: State of the art." *IEEE Communications Surveys and Tutorials*, vol. 17, no. 3, pp. 1649–1678, 2015.

[27] K. Qiu, F. Zhang, and M. Liu, "Visible light communication-based indoor localization using gaussian process," in *Intelligent Robots and Systems (IROS), 2015 IEEE/RSJ International Conference on*. IEEE, 2015, pp. 3125–3130.

[28] M. Yasir, S.-W. Ho, and B. N. Vellambi, "Indoor positioning system using visible light and accelerometer," *Journal of Lightwave Technology*, vol. 32, no. 19, pp. 3306–3316, 2014.

[29] Q. Wang, D. Giustiniano, and D. Puccinelli, "An open source research platform for embedded visible light networking," *IEEE Wireless Communications*, vol. 22, no. 2, pp. 94–100, 2015.

[30] L. Klaver and M. Zuniga, "Shine: A step towards distributed multi-hop visible light communication," in *Mobile Ad Hoc and Sensor Systems (MASS), 2015 IEEE 12th International Conference on*. IEEE, 2015, pp. 235–243.

[31] Philips, "Unlocking the value of retail apps with lighting," http://www.lighting.philips.com/main/systems/themes/led-based-indoor-positioning/white-paper, accessed June 9, 2017.

[32] H.-S. Kim, D.-R. Kim, S.-H. Yang, Y.-H. Son, and S.-K. Han, "An indoor visible light communication positioning system using a rf carrier allocation technique," *Journal of Lightwave Technology*, vol. 31, no. 1, pp. 134–144, 2013.

[33] M. Liu, K. Qiu, F. Che, S. Li, B. Hussain, L. Wu, and C. P. Yue, "Towards indoor localization using visible light communication for consumer electronic devices," in *Intelligent Robots and Systems (IROS 2014), 2014 IEEE/RSJ International Conference on*. IEEE, 2014, pp. 143–148.

[34] L. Jean, Paul, "Jpl's wireless communication reference website," http://www.wirelesscommunication.nl/reference/chaptr06/randacc.htm, accessed June 9, 2017.

[35] "Ieee standard for local and metropolitan area networks–part 15.7: Short-range wireless optical communication using visible light," *IEEE Std 802.15.7-2011*, pp. 1–309, Sept 2011.

[36] C. E. Rasmussen, "Gaussian processes for machine learning," 2006.